Geophysica (2016), 51(1-2), 51–67

Clarification of Pasha Rift Structure in Pasha-Ladoga Basin Based on AMT and Gravity Data

K. Stepanov[1], Kseniya Antashchuk[2] and Alexander Saraev[2]*

[1]CJSC «NPP VIRG-Rudgeophysica», Saint Petersburg, Russia
[2]Institute of the Earth Science, Saint Petersburg State University, Saint Petersburg, Russia

*Corresponding author: Kseniya Antashchuk, antaschuk@list.ru

(Received: April 2016; Accepted: October 2016)

Abstract

Clarification of the Pasha-Ladoga Basin structure was conducted using a joint interpretation of audiomagnetotelluric (AMT) and gravity data. AMT investigations were performed along a regional profile with a length of 86 km, and three additional 10 km profiles within the south-eastern part of the basin. A four-layered geoelectrical model was obtained up to a depth of 2 km according to 2D inversion results of AMT data, and model interpretation enabled determination of the upper and lower boundaries of Riphean rocks in the Ladoga-Pasha Basin. Maximum thickness of the zone of the Riphean deposits was established in the central part of the regional profile, and two conductive zones were determined in the crystalline basement structure; these are probably related to faults and graphitic zones. Joint AMT and gravity data interpretation results clarified a division of the Pasha-Ladoga Basin area and determined two fore deeps and a central linear zone with a trough structure, where the zone is characterized by a maximum thickness of Riphean deposits and corresponds to the linear positive anomaly of the gravity field in a north-western direction. Results of gravity field modeling show that this anomaly relates to dense rocks, which are probably basalts and mafic volcanic rocks, and which have a lower boundary depth of 4–5 km. The structure of this zone and its filling by mafic volcanic rocks can be interpreted as a rift structure, and based on gravity data the rift structure is found to extend to the Ladoga Lake area, with an observed length of about 140 km and a width of 17–25 km. The results obtained in this study allow better definition of the borders and specification of the Pasha structure's rift origin.

Keywords: Pasha-Ladoga Basin, Pasha Rift, audiomagnetotelluric sounding, gravity survey

1 Introduction

The Pasha-Ladoga Basin is located on the border between the Russian Plate and the Fennoscandian Shield and its formation is controlled by the Ladoga-Bothnia zone of deep long-living fractures at the joining zone of the Karelian and the Svekofennian geoblocks (*Amantov*, 2014). MT-MV soundings (*Rokitiansky et al.*, 1979; *Kovtun*, 1989; *Klabukov and Grishin*, 1993; *Zhamaletdinov and Klabukov*, 1993; *Kovtun et al.*, 2011) and seismic investigations (*Isanina et al.*, 2004) have been conducted to study the structure of this deep zone. The thickness of the Earth's crust has thus been estimated, and several deep faults and fractured zones within the Earth's crust have also been described from seismic data. In addition, electromagnetic investigations have permitted

studies of the resistivity structure, and an anomaly of high conductivity in the Earth's crust has been determined at the border between the Karelian and the Svekofennian geoblocks.

The geological structure of the Pasha-Ladoga Basin and the surrounding area has been considered in a number of studies (*Amantov and Spiridonov*, 1989, *Amantov et al.*, 1996; *Stupak and Leshchenko*, 2008; *Kuptsova*, 2012; *Amantov*, 2014). However, the interior structure of the basin has not yet been adequately researched. In the south-eastern part a separate structure, known as Pasha Graben, has been determined in the interior part of the basin using geophysical data (*Amantov and Spiridonov*, 1989, *Amantov et al.,* 1996; *Amantov*, 2014).

A joint interpretation of earthquake-generated converted waves and common depth point (CDP) seismic data obtained along a regional profile of Novaya Ladoga-Oshta has enabled new information to be obtained in relation to the outer crust structure of the Earth in the south-eastern part of the Ladoga area (*Stupak and Leshchenko*, 2008). The earthquake converted waves method has shown that deep faults are associated with faults in the outer Earth's crust. In addition, seismic data have shown that the Riphean valley (the Pasha Graben) is related to the mantle fault zone, and that the basement rocks beneath the valley are composed of mafic and ultramafic intrusions.

The aim of this study is to determine the interior structure of the Pasha-Ladoga Basin according to a joint interpretation of regional gravity data and audiomagnetotelluric soundings (AMT) along a regional profile with a length of 86 km and three additional profiles with a length of 10 km each.

2 Geological setting

The Pasha-Ladoga Basin is part of the widespread rift system lying under the sedimentary cover of the Russian Plate in the western part of the Fennoscandian Shield (*Kuptsova*, 2012). The basin contains Riphean sedimentary and extrusive rocks and extends from the Ladoga Lake area to the south-east. Riphean sediments fill the northern part of the Ladoga Lake sub-bottom, and outcrop in the eastern and western parts of the lake's coast. In the southern and south-eastern parts of the study area, the Riphean rocks are covered by the Vendian-Paleozoic sediments of the East European Platform. Figure 1 shows a geological map of the pre-platform deposits.

According to well data, the Riphean deposits in the Pasha-Ladoga Basin have a maximum thickness of 450 m and are represented by sandstones with siltstone interlayers and flood basalts. Basal units consist of gravel conglomerates, redbed sandstones, and cover with an angular unconformity the Archean-Proterozoic basement and Riphean rapakivi granites. The sedimentary and extrusive rocks of the Pasha-Ladoga Basin are intruded by gabbro-dolerite sills. The age of the Riphean basin formation has been dated according to flood basalt as 1499 ± 68 Ma (*Bagdanov et al.,* 2003), and the intrusion age of the largest Valaam sill as 1459 ± 3 Ma (*Rämö et al.*, 2001).

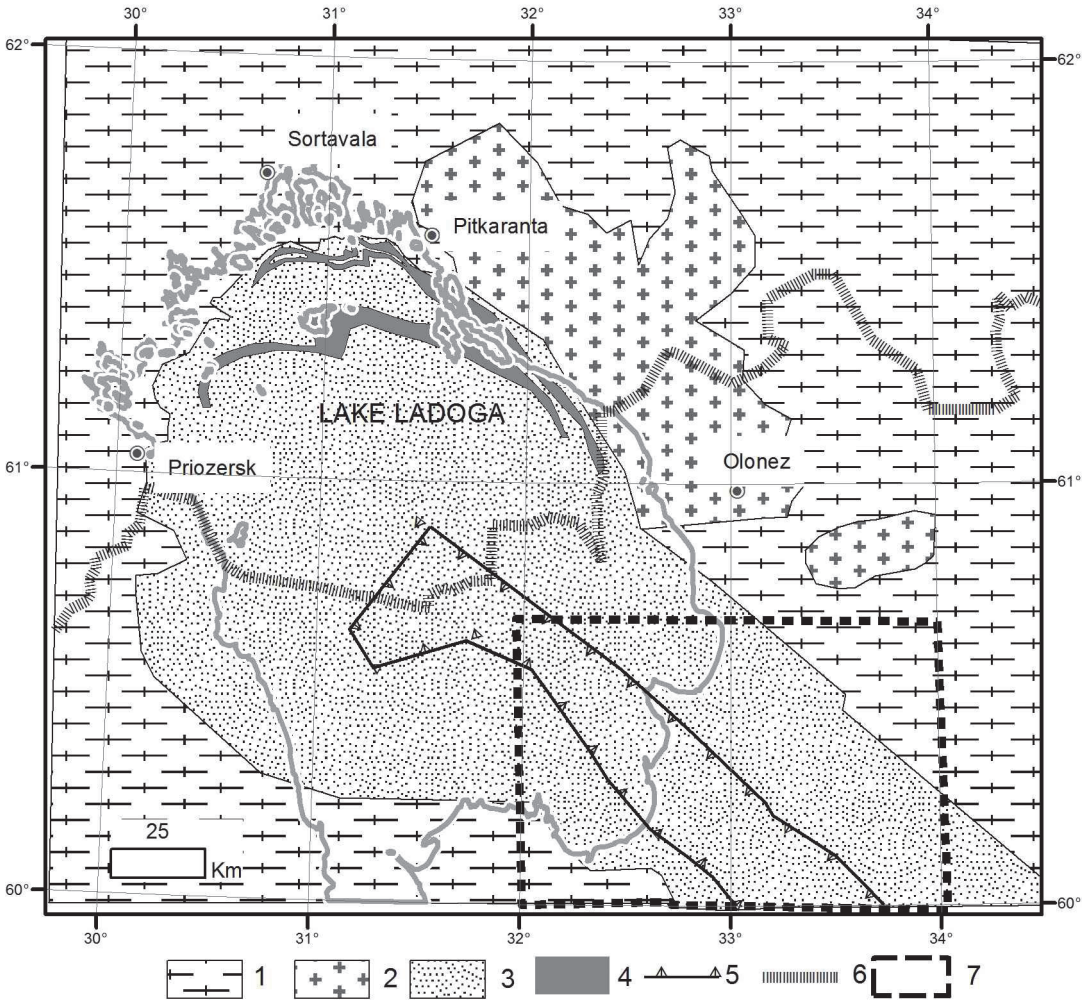

Fig. 1. Geological map of pre-platform deposits and location of Pasha-Ladoga Basin. Modified after *Kuptsova*, 2012

1. Archean-Proterozoic metasedimentary and metavolcanic rocks of the crystalline basement; 2. Riphean rapakivi granites; 3. Riphean sedimentary and volcanic rocks of the Pasha-Ladoga Basin; 4. Riphean sills (basalts, gabbro-dolerites); 5. Borders of Pasha rift zone according to this study; 6. Northern border of Vendian-Paleozoic sedimentary cover (sandstones, siltstones, clays, gravel conglomerates, argillites); 7 – Area of study.

Gravity and magnetic data analysis and a previous study of *Amantov* (2014) have determined that the geological structures in the study area have south-east strike direction. Figures 2 and 3 show the Bouguer gravity map with mapped faults and a rose-diagram of the fault strike, respectively.

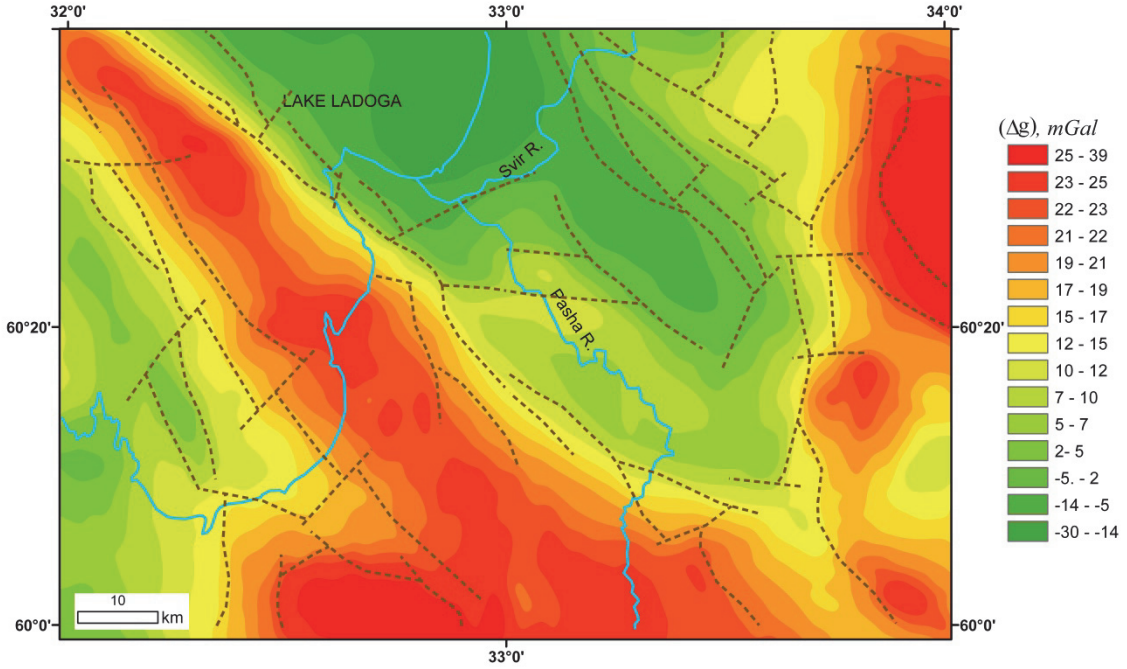

Fig. 2. Bouguer gravity map and mapped faults (brown dotted lines).

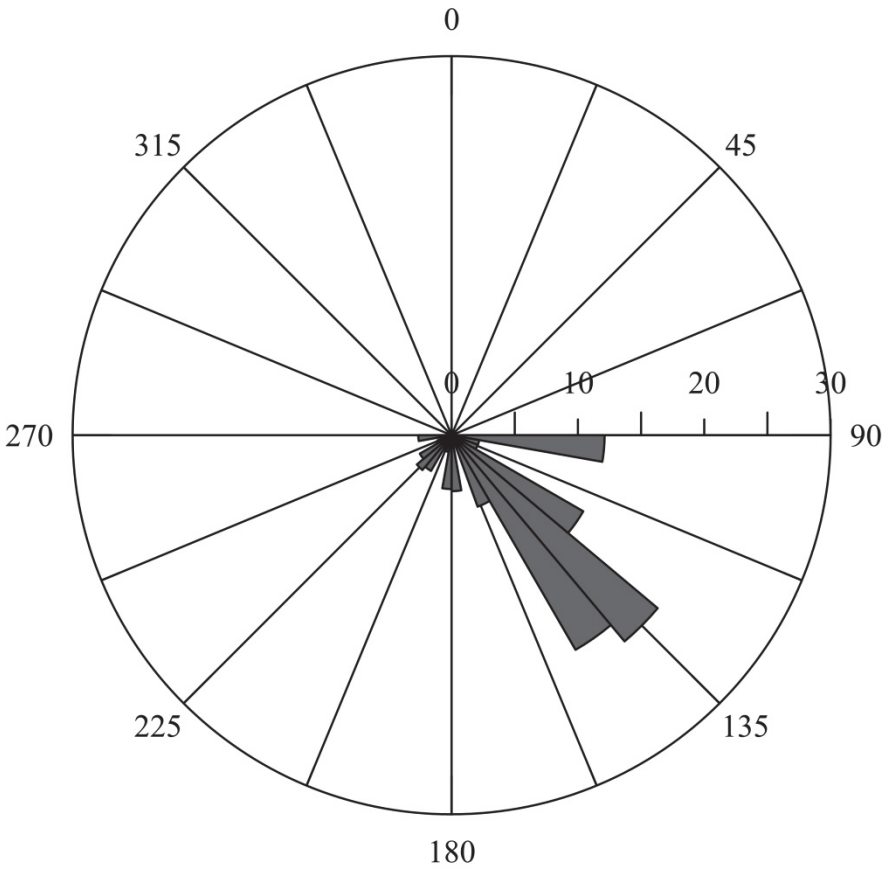

Fig. 3. The rose-diagram of the faults strikes in the investigated area.

3 AMT data

3.1 AMT data acquisition and processing technique

AMT data were acquired from 121 stations; 87 of these stations belong to the regional profile in a north-east direction (Line A-B), 13 stations are situated along the cross profile (Line-1), and 21 stations are located along two parallel profiles (Line-2 and Line-3). Figure 4 shows the survey area. There is an average distance of 1 km between stations on each profile. AMT measurements were conducted using the ACF-4M system (*Saraev et al.*, 2011), and the measurement array at each station provided a record of electric (E) and magnetic (H) horizontal electromagnetic field components in directions magnetic north (Ex and Hx) and east (Ey and Hy). The electric antennae were approximately 100 m long. Recorders were synchronized during measurements by GPS so that it was possible to apply a remote reference algorithm to calculate the impedance tensor (*Gamble et al*., 1979). Each station in the study area was remotely referenced using a station situated approximately 30 km away from it. Measurements at each station were conducted using two bands (D1 and D3) with different sampling frequencies: measurement times using band D1 (0.1–40 Hz, sampling frequency 160 Hz) and band D3 (1–1000 Hz, sampling frequency 3200 Hz) were 2–3 hours and 20 minutes, respectively.

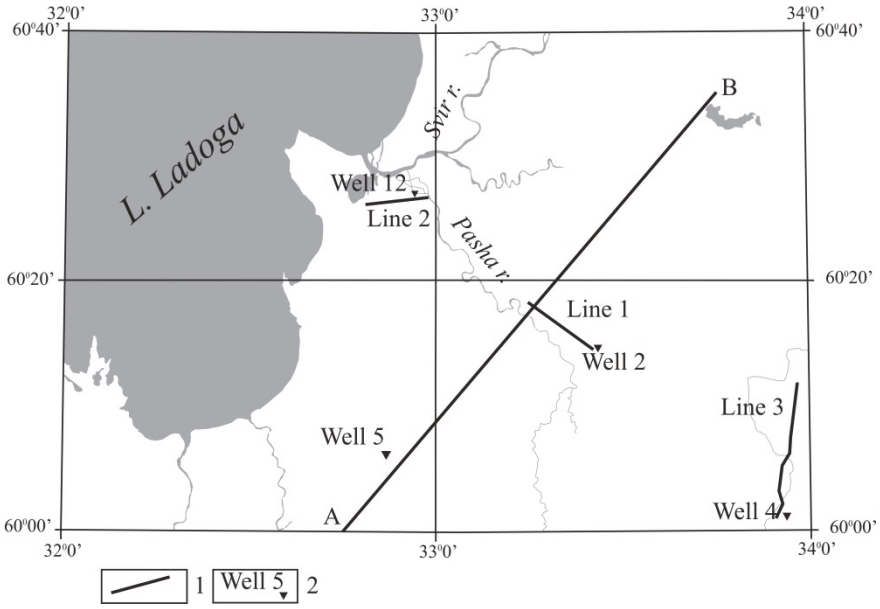

Fig. 4. Location map of (1) AMT sounding lines, and (2) wells.

AMT field data were processed using SM+ software, which is included in the ACF-4M set (*Saraev et al.*, 2011). The entire frequency range (0.1–1000 Hz) was divided into several adjacent frequency bands, and each sounding curve had approximately 40 points per decade. Spectral analysis of the time series was carried out in each frequency band using Fast Fourier Transformation (FFT) and the Blackman window function in order to estimate the power-spectra density (PSD) of measured signals. A robust regression analysis was then applied to these data, and estimations of

impedance tensor elements were obtained. In addition, the Gamble reference method (*Gamble et al.*, 1979) and Huber robust regression (GM-estimator) with biquadrate loss-function were used for the bias estimation and dispersion reduction (*Chave and Thomson*, 2004; *Huber*, 1964; *Huber*, 1981, *Wilcox*, 2005).

3.2 AMT data analysis and inversion results

After processing, AMT data analysis and inversion were then conducted using the ZondMT software (www.zond-geo.com) including following operations: rotate the impedance tensor, calculate and display dimensionality parameters (skew, strike, polar diagrams of impedance and phase tensors), and implement 1D and 2D magnetotelluric data inversion.

Strike direction was determined using the Groom and Bailey (G-B) impedance tensor decomposition approach (*Groom and Bailey*, 1989), and rose diagrams were used to determine the G-B predominant strike direction for all stations on the Line A-B, both in the entire frequency band and in the frequency range of 0.1–10 Hz and 10–400 Hz (Fig. 5). The diagrams show that the major strike direction for all frequencies is approximatly 135°–150°, and that the strongest distorsion of strike values is observed in the low-frequency range. This is considered to be related to the "dead band" effect that causes an decrease in data quality during these periods. However, at these frequencies the strike is mainly directed to the south-east, and as described in the geology section in this study, the major structure and faults of the area lie close to a south-easterly direction, and therefore the AMT data were rotated to approximately 45°. After rotation, the xy component was found to correspond to the TM polarization mode, in which electric currents flow across the faults, while the yx component corresponds to the TE mode, where electric currents flow along the faults. These data were then used in the following analysis.

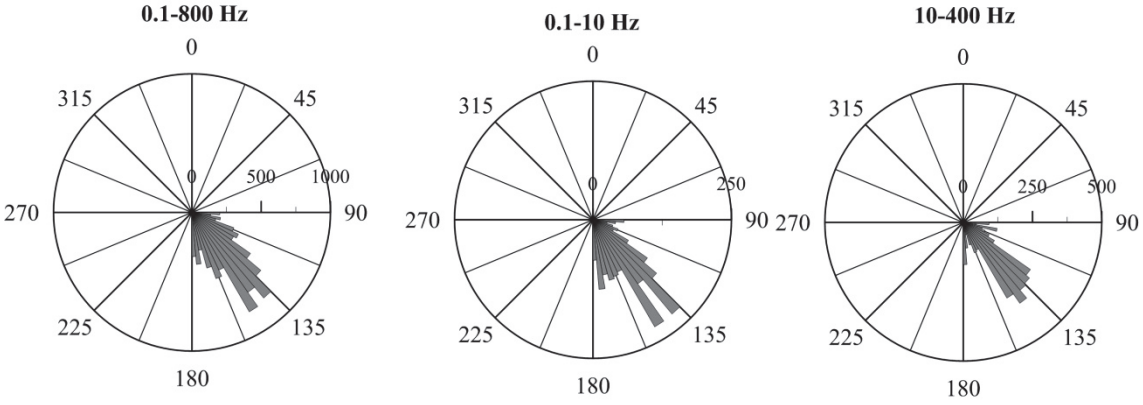

Fig. 5. Rose-diagrms calculated using Groom and Bailey method for frequency ranges 0.1–800, 0.1–10 and 10–400 Hz for Line A-B.

Figure 6(a) shows pseudo sections of apparent resistivity and the impedance phase along Line A-B for both polarizations. Figure 7 then shows the apparent resistivity,

impedance phase curves, and skew for several stations with a typical curved behaviour. The skew can be written (*Swift*, 1967) as:

$$skew = \frac{|z_{xx} + z_{yy}|}{|z_{xx} - z_{yy}|}\ ; \tag{1}$$

where Z_{xx}, Z_{yy} are the diagonal and Z_{xy}, Z_{yx} are the off-diagonal elements of the impedance tensor. The skew values are used to evaluate whether electrical structures below the AMT sites deviated from 1- or 2-dimensional (1D or 2D). When skew values is less than 0.2 in low-noise conditions then a 1D or 2D model was valid.

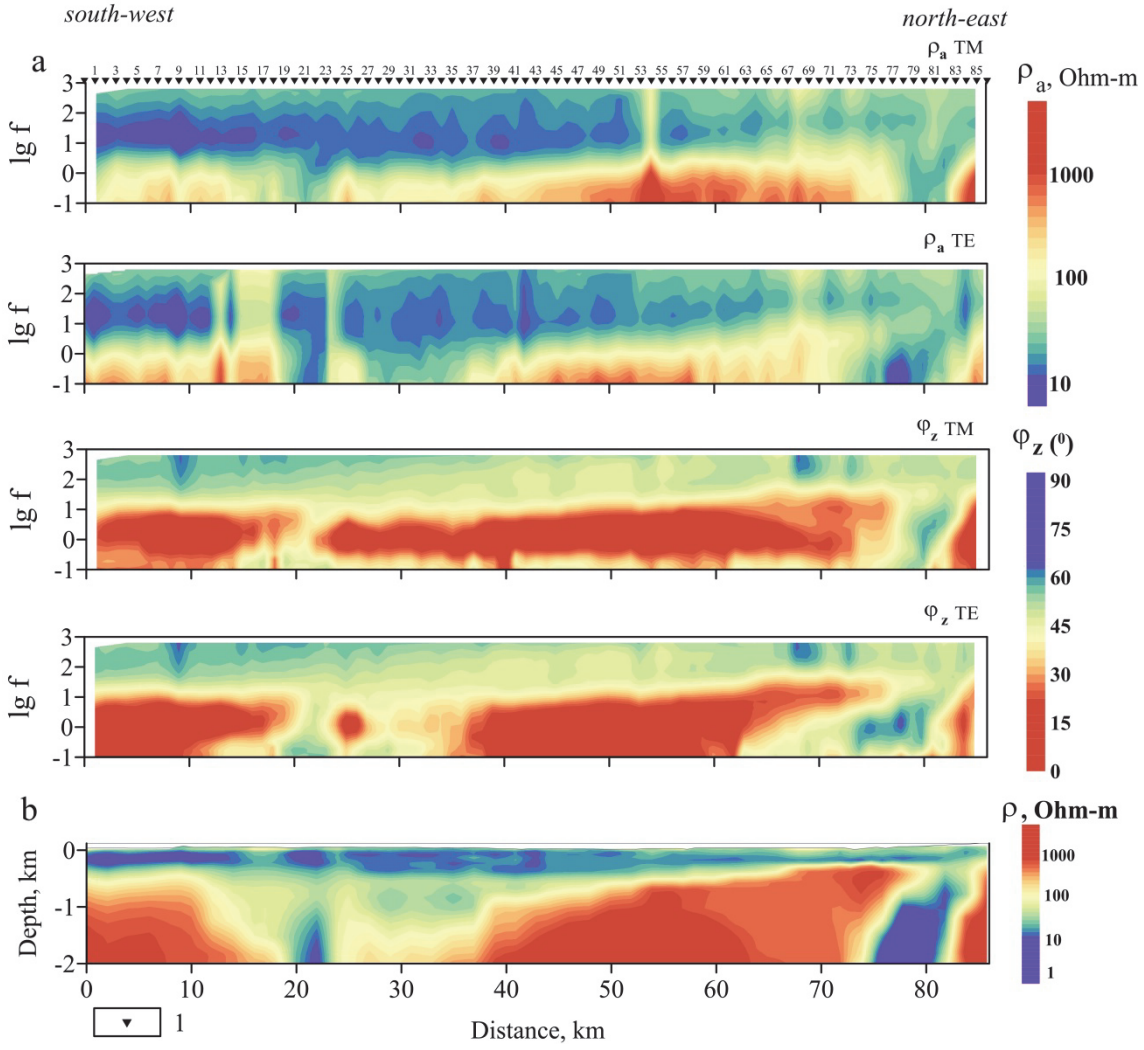

Fig. 6. (a) Pseudo sections of: apparent resistivity (ρ_a) and impedance phase (φ_z) for TM and TE polarizations; and (b) geoelectric model according to AMT data 2D inversion along Line A-B. 1. AMT stations.

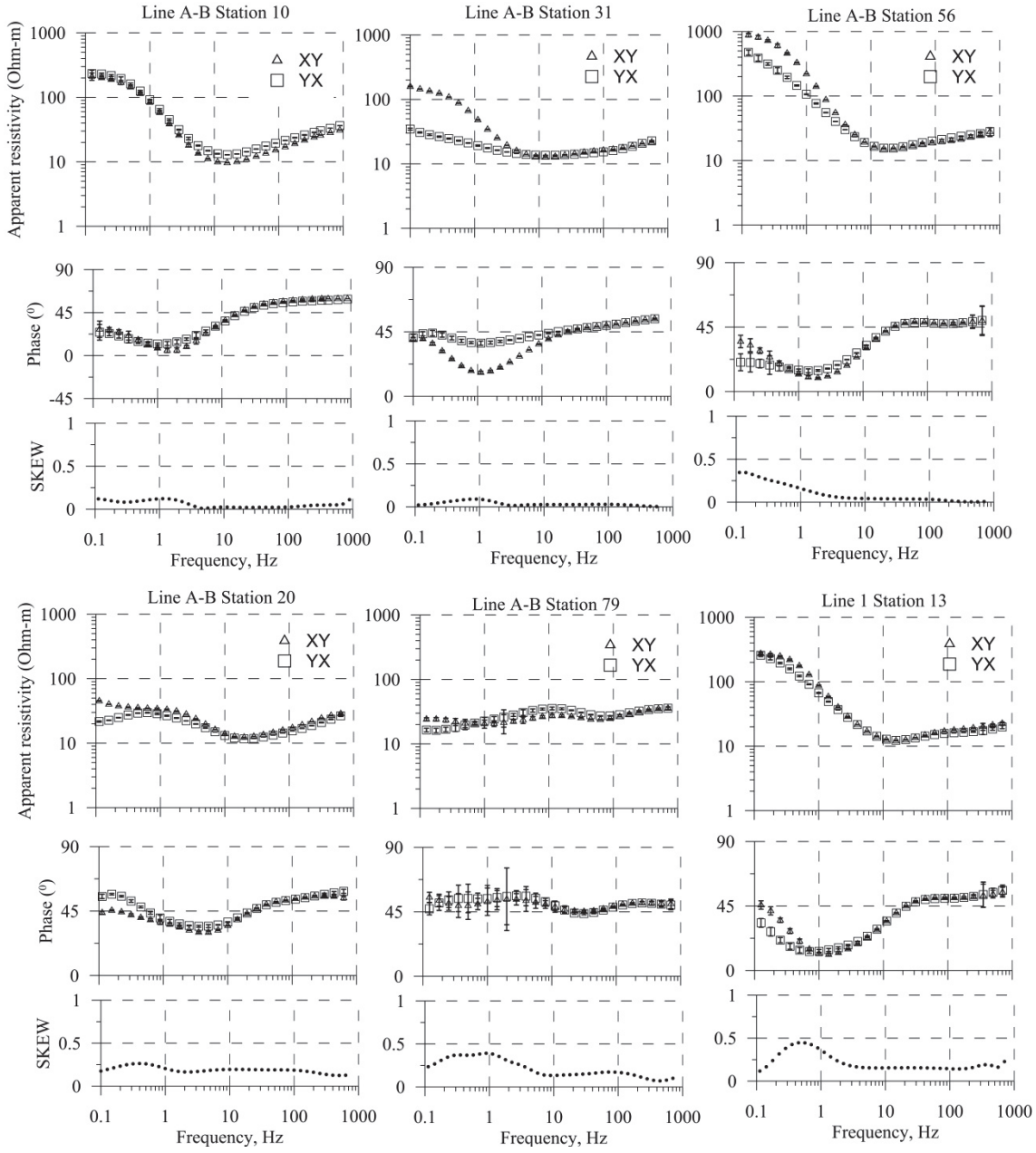

Fig. 7. Apparent resistivity and impedance phase curve examples for TM (xy) and TE (yx) modes and skew for several stations; stations are named in accordance with their distance along the profile in km.

Line A-B can be divided into several sections based on the features of the sounding curve. For stations 0–14, the apparent resistivity and impedance phase curves have a similar shape and represent the HA-type. In addition, the skew values in the frequency range 3–300 Hz are close to zero, and at low- and high-frequencies they are less than 0.2. Therefore, based on these results we can assume that the structure of this area is close to that of a 1D layered model.

For central and north-eastern parts along Line A-B (Stations 15–77 and 83–86), the sounding curves are also of an HA-type, and are congruent at frequencies higher than 10 Hz and split at low-frequencies. However, an increase in the minimum position of the frequency curve can be observed from south-west to north-east, which indicates a

decrease in the thickness of the upper low-resistivity layer in this direction. For stations in the 15–20 interval, the skew values in the entire frequency band are about 0.25, which indicates the existence of a 2D or 3D structure in this area. For other stations, the skew values are only greater than 0.2 for frequencies where the curves split and there is a high noise level, which could also be the cause of the increasing skew value. Thus, 2D inhomogenity effects are observed for deep structures.

The anomalous behavior of sounding curves is observed at stations 77–83, where curves are congruent at frequencies higher than 100 Hz and split at lower ones. The curves have HK-type, and the skew values lie between 0.2 and 0.3, thereby indicating a 2D or 3D structure.

Station 54 for TM polarization and stations 13, 15, 16, 17, 18, 69 for TE polarization show strong static-shift effects, and thus a static-shift correction was implemented automatically during 2D inversion.

The inversion procedure involved two stages. In the first stage we used effective curves of apparent resistivity, ρ_{eff}, and an impedance phase, φ_{eff}, for 1D inversion using ZondMT software. These curves were calculated according to (*Berdichevsky and Dmitriev*, 2009),

$$\begin{aligned} \lg \rho_{eff} &= \frac{\lg \rho_{xy} + \lg \rho_{yx}}{2}; \\ \varphi_{eff} &= \frac{\varphi_{xy} + \varphi_{yx}}{2}, \end{aligned} \tag{2}$$

where ρ_{xy}, ρ_{yx} are the apparent resistivities, and φ_{xy}, φ_{yx} are the impedance phases in the xy and yx directions, respectively.

Occam inversion (*Constable et al.*, 1987) was then conducted with a 15-layer start model. Results showed that for sites with a 1D structure (stations 0–14) and with a 1D structure of a shallow section, the route mean square (RMS) error value did not exceed 8 % after 50 iterations, whereas at other sites (station intervals 15–20 and 77–83) it reached 20–30 %.

Well data were also used in 1D inversions (well positions are shown in Fig. 4), and an example of geoelectrical model fitting is shown in Fig. 8 for Stations 10 and 42 of Line A-B, which are located near Wells 5 and 2, respectively. The geoelecric model obtained has a positive correlation with well data. Vendian-Paleozoic deposits, which are composed mainly of clays, are characterised by resestivity values of about 10 Ω·m. A low thickness layer with resistivity values of about 100 Ω·m is observed in the upper part of the model, which corresponds to sandstones and limestones. Riphean sandstones with basalt interlayers are also characterised by resistivity values of about 100 Ω·m, and increasing resistivity of up to 1000 Ω·m is observed in the bottom part of the model, which corresponds to Arhean-Proterozoic rocks of the crystalline basement.

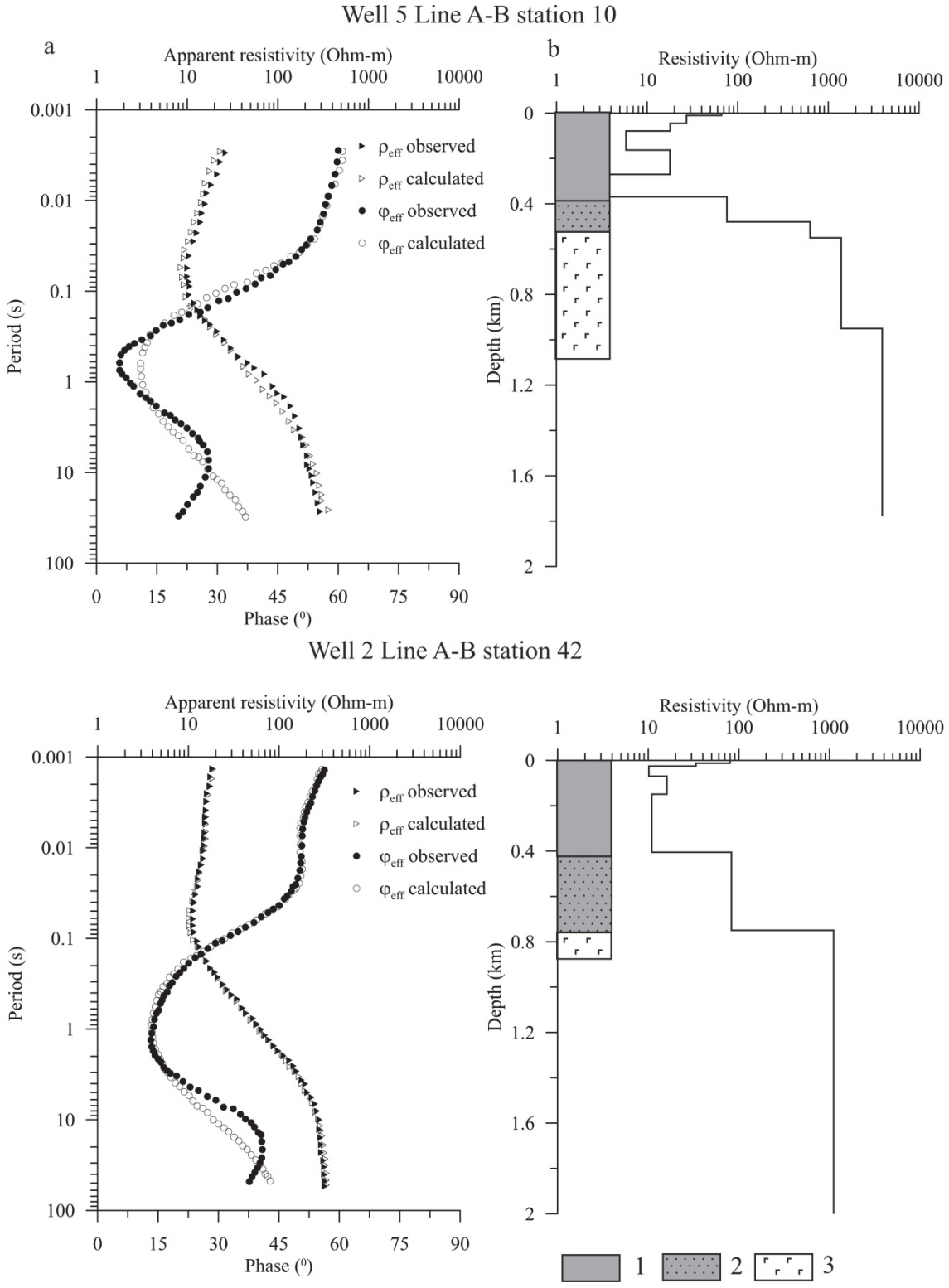

Fig. 8. 1D inversion resuls of AMT data for stations near Wells 2 and 5 (well positions are shown in Fig. 3). a) Observed and calculated AMT effective curves; b) well section and fitted electrical model according to 1D inversion of AMT data. 1. Vendian-Paleosoic seimentary deposits; 2. Riphean sandstones with basalt interlayers; 3. Arhean-Proterosoic crystalline basement (gabbro).

The geoelectric model obtained for stations with a small RMS value (less than 8 %) was applied as the initial model in the 2D inversion. The Occam inversion

(*deGroot-Hedlin and Constable*, 1990) algorithm was used for the 2D inversion. We applied the joint TE + TM inversion because it allowed inclusion of both polarization information, which is superior for medium with horizontal heterogeneities. The model mesh was constructed with an incremental factor of 1.2, and the first layer thickness was 10 m. The model included 24 layers and was calculated up to a depth of 3.92 km. We aimed to determine the vertical heterogeneity, and thus we did not assign prevalent smoothing in either a vertical or horizontal direction; in the ZondMT software this corresponds to a smoothing ratio value of 1. The regularization (Tikhonov) parameter controls the trade-off between fitting the AMT data and producing a spatially smooth model. In the ZondMT software it can be set in range from 0.005 to 0.5. Than higher this value than more smoothed model will be calculated, which is adequate for noisy data. For the not disturbed data the Tikhonov parameter is usually set between 0.005–0.01. The value of the Tikhonov regularization parameter was 0.02 because AMT data have a low noise level. The RMS error value of the resistivity model obtained was 2.8%.

The geoelectrical model along Line A-B was obtained according to a 2D inversion of AMT data (Fig. 6b). Four layers are determined in a depth range of 50–2000 m. The first shallow layer (up to 100 m depth) is observed for only some parts of Line A-B, and a small increase in the resistivity value of up to 100 Ω·m is established for this layer. The second layer is characterized by low resistivity values (1–50 Ω·m) and a constant thickness along the investigated profile. The third layer has resistivity values of 50–500 Ω·m, which are observed from the south-western end of Line A-B to Station 68. The resistivity of the fourth layer exceeds 500 Ω·m. However, the geoelectric model is complicated by vertical heterogeneities of low resistivity values (less than 10 Ω·m) at Stations 20–24 and 75–83.

Well data and available geological information were used in the interpretation of the geoelectric model. The second layer of low resistivity was found to correspond to Vendian-Paleozoic sedimentary rocks mainly consisting of clay stones. Lenticular high resistive zones in the upper part of this layer represent the Paleozoic sandstones and limestones. The Vendian-Paleozoic deposits overlay older rocks in the study area, and their thicknesses vary from 250 m in the north-western part of Line A-B, increasing in its central part to 450 m, and in the south-eastern part reaching 300 m. The third layer consists of Riphean sandstones, siltstones, and extrusive rocks of the Pasha-Ladoga Basin.

The data obtained in this study allowed us to determine the upper and lower boundaries of Riphean rocks and the geological features of both the Pasha-Ladoga Basin and the crystalline basement structure along Line A–B. Riphean deposits were observed at Station 68, where their lower boundary is located at 300 m. In a south-west direction towards Station 55, the lower boundary dips smoothly in small increments, and after reaching a depth of 600 m it then dips more steeply at Stations 38–55 up to a depth of 900 m. A trough structure with steep walls is observed at Stations 10–38, where the thickness of the central part of Riphean deposits is more than 2 km. In addition, a low resistive vertical zone connected with a fault is determined at Station 22.

The fourth layer corresponds to high resistive rocks of the Archean-Proterozoic crystalline basement; in this layer the conductive zone is observed at Stations 75–82 and is probably in relation to the flat dipping fault and graphitic zone in the Low-Proterozoic schists (as graphitic schists of the Low-Proterozoic Pitkaranta Suite are known in the northern and eastern Ladoga regions) (*Stepanov et al.*, 2004, *Kotova et al*., 2011).

4 Technique used for density distribution modeling

Density distribution modeling was implemented using GM-SYS software (Geosoft Inc.) and the Bouguer gravity map 1:200000 from the Federal Database of gravity and magnetic data «GRAVIMAG» (VIRG «Rudgeophysica», Saint-Petersburg, Russia) (Fig. 2). Gravity field data were obtained along investigated profiles from an area with a grid of 200 x 200 m. The coincidence of observed and calculated gravity field curves was used as quality criterion in the obtained density model.

Shape of polygons was set based on the AMT (Fig. 6b), well data, and geology. Density values were set for each of the model polygons according to a laboratory-based core study for neighboring areas. The following density values were specified for different rocks in the area investigated: Vendian-Paleozoic sediments 2.4 g/cm^3; Riphean sandstones with a basalt interlayer 2.6–2.7 g/cm^3; Riphean basalts and dolerites 2.9 g/cm^3; Riphean rapakivi granites 2.6 g/cm^3; gabbro 2.9 g/cm^3; Low-Proterozoic shields and gneisses 2.75–2.78 g/cm^3; Archean gneisses and migmatites 2.75 g/cm^3; Archean amphibolites 2.83 g/cm^3.

5 Joint geological interpretation results.

The geoelectrical model obtained along Line A-B was used for the gravity field modeling and geological model construction (Fig. 9c). According to the results of modeling, gravity field anomalies at sites of the lower boundary of flat bedding Riphean deposits were determined by heterogeneities in the crystalline basement, and the trough structure allocated by AMT data corresponds to the gravity positive anomaly. The results of the modeling have shown that this anomaly is caused by dense rocks (density 2.9 g/cm^3), and is thus probably represented by Riphean basalts and mafic volcanic rocks. The lower boundary of these rocks lies at a depth of 4 km.

The positive gravity anomaly corresponding with the trough structure at the Line A-B has a linear behavior and extends to the Ladoga Lake area (Fig. 10). Gravity field modeling was carried out along Line C-D (position is shown in Fig. 10) on the extension of this anomaly, and the geological model obtained conforms to the model along Line A-B and confirms that a trough structure filled with mafic rocks extends in a northwesterly direction to the area of Ladoga Lake. The lower boundary of basic rocks lies at a depth of 5 km in this model (Fig. 11).

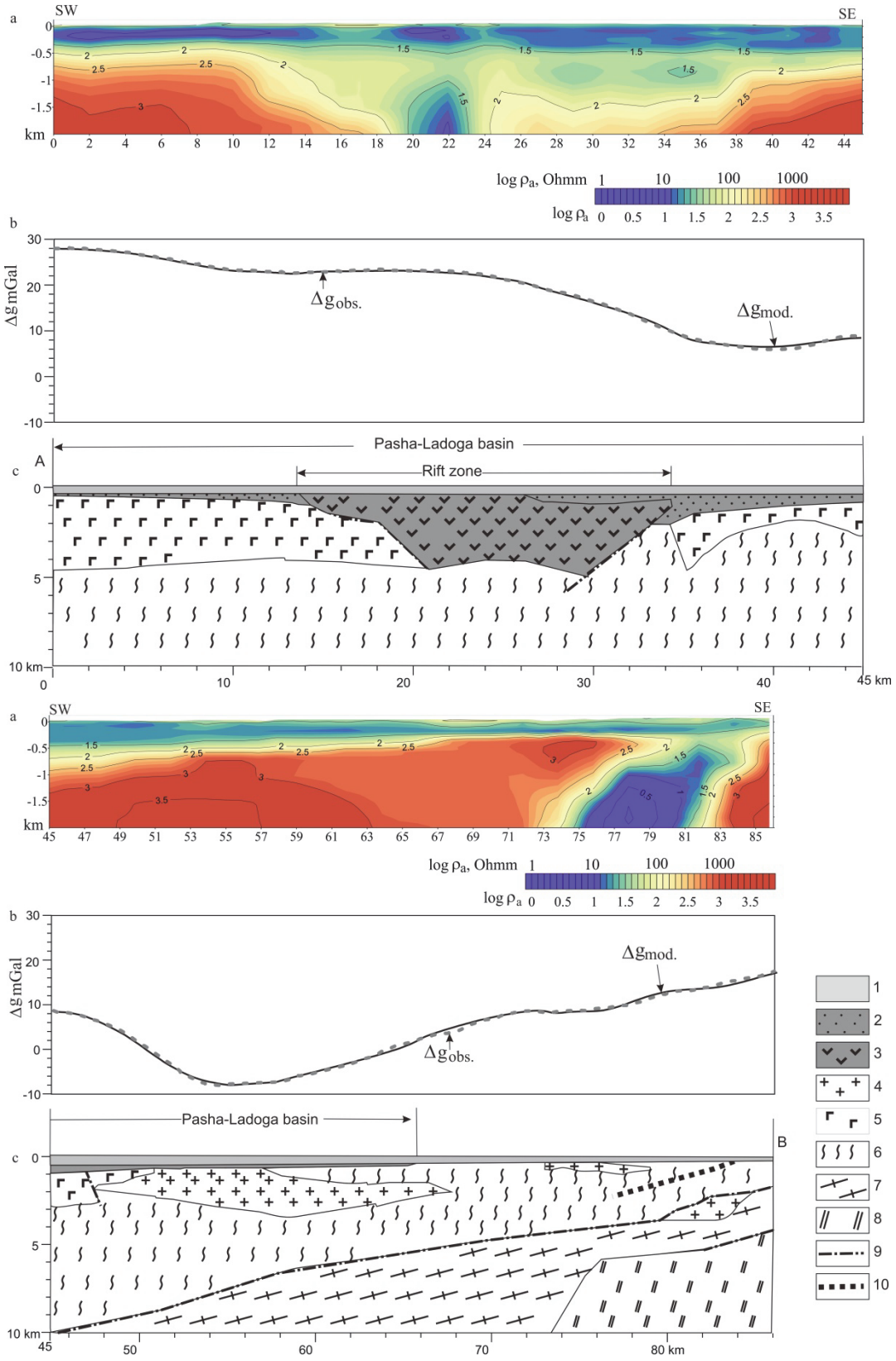

Fig. 9. (a) Geoelectrical model; (b) plots of observed ($\Delta g_{obs.}$) and calculated ($\Delta g_{mod.}$) gravity fields; and (c) geological model (c) along Line A-B. Ratio of horizontal and vertical scales is 1:3 for geoelectrical model.

1. Vendian-Paleozoic sedimentary rocks; 2. Riphean sandstones with basalt interlayers; 3. Riphean basalts and dolerites; 4. Riphean rapakivi granites; 5. Gabbro; 6. Low-Proterozoic schists and gneisses; 7. Archean gneisses and migmatites; 8. Archean amphibolites; 9. Faults; 10. Faults marked by low resistive zones.

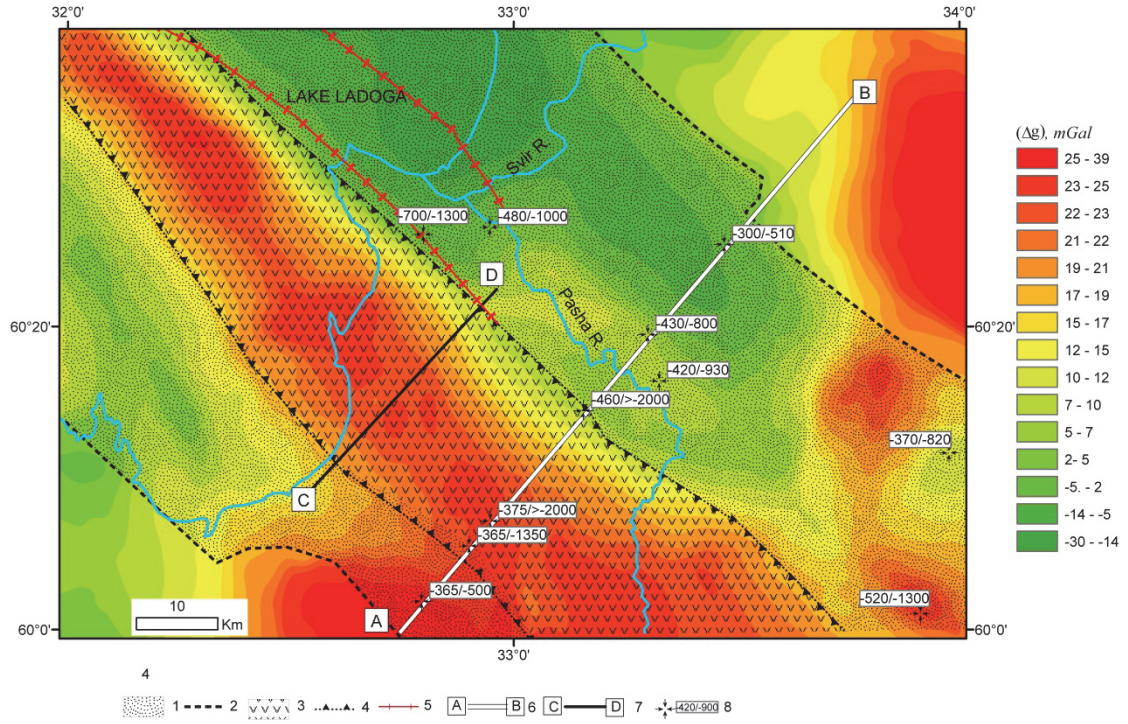

Fig. 10. Bouguer gravity map and tectonic map of Pasha-Ladoga Basin.
1. Fore deeps; 2. Borders of Pasha-Ladoga Basin; 3 and 4. Pasha rift and boundaries; 5. Part of Pasha graben according to Amantov et al., 1996; 6. Line of AMT and density modeling; 7. Line of density modeling; 8. Depth values of upper and lower boundaries of Riphean deposits by AMT data.

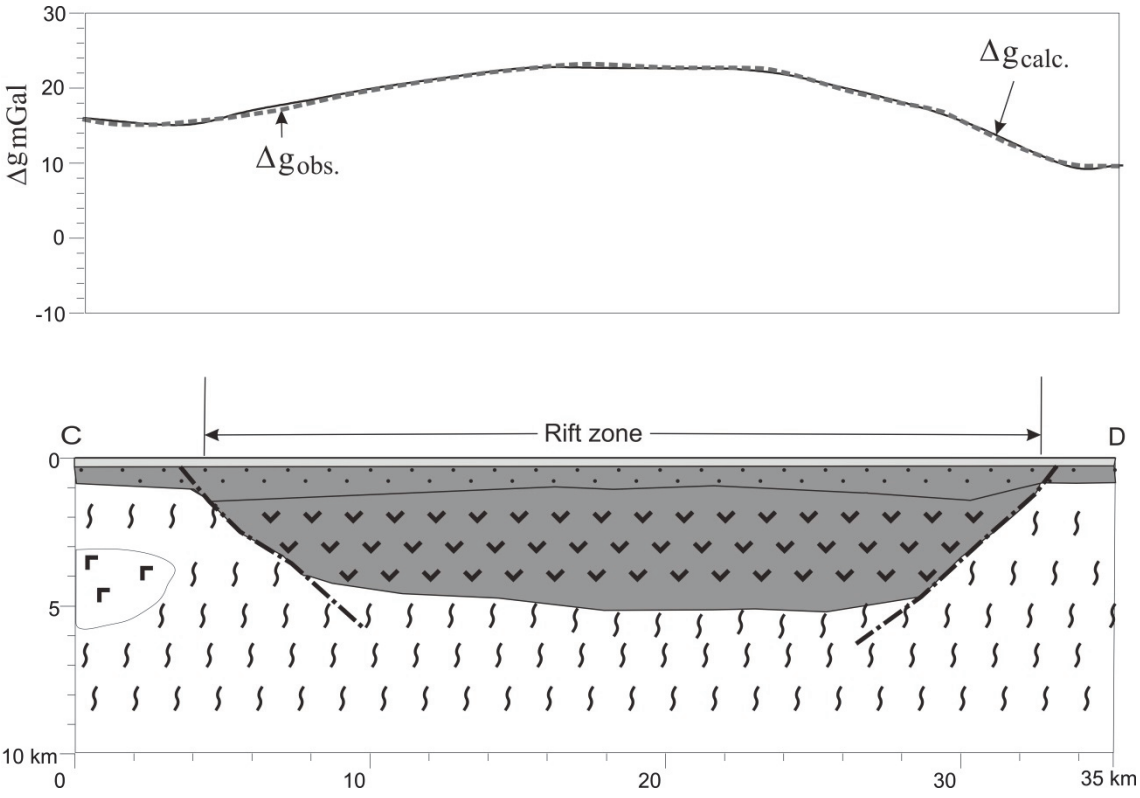

Fig. 11. (a) Graphics for observed ($\Delta g_{obs.}$) and calculated ($\Delta g_{mod.}$) gravity fields and (b) geological model along Line C–D (position shown in Fig. 10). Legend shown in Fig. 9.

The results of joint interpretation allow us to divide the Pasha-Ladoga Basin area into different sections (Fig. 10). Two fore deeps and a central linear zone with a trough structure are determined according to geological data and the behavior of geophysical fields. The upper and lower contacts of Riphean deposits in the north-eastern fore deep, obtained along the additional AMT profiles (Line-1, Line-2 and Line-3 in Fig. 4), confirm the increasing thickness of these deposits in a south-westerly direction. The principal feature of the central linear zone is the gravity field, which is a linear positive anomaly in a north-westerly direction, and is crossed by Lines A-B and C-D in its south-eastern part. The structure of this zone, and the fact that it is filled with mafic volcanic rocks, could allow it to be interpreted as a rift structure. This assumption is also inferred from the gravity data. The zone extends to the Ladoga Lake area (Fig. 11), has an observed length of about 140 km, and a width of 17–25 km.

The Pasha Graben boundaries determined during previous investigations using geophysical data (*Amantov et al.*, 1996; *Amantov*, 2014) join the rift structure in the north-east and have the same strike direction. However, previous researchers have (*Amantov et al.*, 1996) noted that the borders are assumptive. AMT data, and the results of density modeling, show the maximum thickness of the Riphean deposits outside the Pasha Graben borders determined in previous investigations (Fig. 10). Thus, it is confirmed that this study allows an accurate determination of borders, and the ability to specify the rift origin of the Pasha structure.

6 Conclusions

New data pertaining to the south-western part of the Pasha-Ladoga Basin structure are obtained according to joint AMT and gravity data interpretation. The AMT results allow determination of the upper and lower boundaries of Riphean rocks and the distribution of a trough structure. The use of gravity field modeling determines this to be a structure lying in a north-westerly direction. The structure is composed of heavy rocks that are probably basalts and mafic volcanic rocks. The results obtained enable a more accurate definition of the borders of the Pasha structure, and allow us to specify its rift origin.

Acknowledgments

This study was supported by the Center for Geo-Environmental Research and Modeling (GEOMODEL) of Research park of St.Petersburg State University. Authors are grateful to Alex Kaminsky (www.zond-geo.com) for the permission of using the MT data analysis and inversion software ZondMT. Authors appreciate very much two anonymous reviewers for their constructive remarks and suggestions.

References

Amantov, A.V., 2014. The geology of the Pre-Quaternary deposits and the tectonic of the Ladoga Lake. *Regional geology and metallogeny,* **58**, 22–23. (In Russian)

Amantov, A., I. Laitakari and Ye. Poroshin, 1996. Jotnian and Postjotnian: sandstones and diabases in the sorroundings of the Gulf of Finland. Explanation to the Map of Precambrian basement of the Gulf of Finland and sorrounding area 1:1 million, Geological survey of Finland, Special Paper 21, 99–114.

Amantov, A.V. and M.A. Spiridonov, 1989. Geology of the Ladoga Lake. *Soviet geology,* **4**, 83–86. (In Russian)

Bagdanov, Y.B., V.V. Savatenkov, V.V. Ivannikov, and D.A. Frank-Kamenetsky, 2003. Isotopic age of volcanites of the Salmi suite of the Riphean. *Isotopic geochronology for solution of problems of geodynamics and ore genesis*, Saint Petersburg, Nauka, 71–72 (In Russian)

Berdichevsky, M.N. and V.I. Dmitriev, 2008. Models and methods of magnetotellurics. Springer-Verlag Berlin, Heidelberg.

Chave, A.D. and D.J. Thomson, 2004. Bounded influence estimation of magnetotelluric response functions. *Geophysical Journal International*, **157**, 988–1006.

Constable, S.C., R.L. Parker and C.G. Constable, 1987. Occam's inversion: A practical algorithm for generating smooth models from electromagnetic sounding data. *Geophysics*, **Vol. 52**, **3**, 289–300.

deGroot-Hedlin, C. and S. Constable, 1990. Occam's inversion to generate smooth, twodimensional models from magnetotelluric data. *Geophysics*, **Vol. 55**, **12**, 1613–1624.

Gamble, T.D., W.M. Goubau and J. Clarke, 1979. Error analysis for remote reference magnetotellurics. *Geophysics*, **44**, 959–968.

Groom, R.W. and R.C. Bailey, 1989. Decomposition of magnetotelluric impedance tensors in the presence of local three-dimensional galvanic distortion. *Journal of Geophysical Research*, **94**, 1913–1925.

Huber, P., 1964. Robust estimation of a location parameter. *The Annals of Mathematical Statistics*, **35**, 73–101.

Huber, P.J.,1981. Robust statistics. John Wiley and Sons, Inc.

Isanina, E.V., N.A. Krupnova and N.V. Sharov, 2004. Seismic investigations by the earthquake converted wave method at the south of Karelia. Deep structure and seismicity of the Karelian region and its margins, Edited by N.V. Sharov, Karelian research center RAS, 60–69. (In Russian)

Klabukov, B.N. and A.S. Grishin, 1993. The association between conductivity and deep structure of the lithosphere of the south-eastern part of the Baltic Shield. Problems of the Precambrian geology of Karelia, Petrozavodsk, 107–117. (In Russian)

Kovtun, A.A., 1989. The structure of the Earth crust and upper mantle at the northwestern part of the Eastern-Europe Plate according to magnetotelluric data. Leningrad State University, Leningrad. (In Russian)

Kovtun, A.A., I.L. Vardaniants and N.I. Uspensky, 2011. Comparision of seismic and geoelectric models for Ladoga-Bothnia anomalous zone. *Problems of geophysics*, **44,** (*The scientific papers of SPbU*, **444**), 124–132. (In Russian)

Kotova, I.K., F.A. Gordon and S.R. Kotov, 2011. Structure and composition of the Pitkaranta suite rocks in the area of stratiform sulfide-skarnoid mineralization (North-East frame of Impilachti dome, Northern Ladoga coast). *Vestnik St. Petersburg University*, **Vol**. **7**, **4**. 28–49. (In Russian)

Kuptsova, A.V., 2012. Geological setting and evolution of the Riphean uraniferous basins: Pasha-Ladoga, East Anabar and Atabaska. PhD thesis, Saint Petersburg State University, Saint Petersburg. (In Russian)

Rämö, O.T., I. Mänttäri, M. Vaasjoki, B.G.J. Upton. and L. Sviridenko, 2001. Age and significance of Mesoproterozoic CFB magmatism, Lake Ladoga region, NW Russia. Geological Society of America, Abstracts with Programs 33(6), A-139.

Rokitiansky, I.I., N.D. Vasin and M.I. Golod, 1979. Electric conductivity anomaly in the south Karelia. *Geophysical papers of the AS USSR*, **Vol**. **89**, Kiev. 35–36. (In Russian)

Saraev, A.K., K.M. Antashchuk, M.I. Pertel, I.S. Eremin, V.B. Golovenko and K.A. Larionov, 2011. The software-hardware system of audiomagnetotelluric sounding ACF-4M. The V Russian Workshop in the name M.N. Berdichevky and L.L. Vanian of the electromagnetic soundings of the Earth (EMS-2011), Saint-Petersburg. (In Russian)

Stepanov, K.I., D.M. Sanin and G.N. Sanina, 2004. Explanation to the State geological map of the Russian Federation 1:200000 sheets P-35-XXIV, P-36-XIX. The 2nd edition. Saint Petersburg. (In Russian)

Stupak, V.M. and N.V. Leshchenko, 2008. Results of the joint interpretation of the earthquake converted waves and CDP seismic data in the south-eastern Fennoscandia, *The seismic prospecting technologies*, **2**. 48–52. (In Russian)

Swift, C.M., 1967, A magnetotelluric investigation of electrical conductivity anomaly in the southwestern United States. PhD Thesis Massachusetts Institute of Technology, Cambridge, MA.

Wilcox, R.R., 2005. Introduction to robust estimation and hypothesis testing. The 2nd edition, Elsevier Academic Press, 429–437.

Zhamaletdinov, A.A. and B.N. Klabukov, 1993. The conductivity anomaly in the consolidated Earth crust. The Karelian-Kola region. The lithosphere structure of the Baltic Shield, National geophysical committee of RAS. (In Russian)